University of Pennsylvania
ScholarlyCommons

Departmental Papers (ESE) | Department of Electrical & Systems Engineering

7-12-2016

Sensor-Based Reactive Navigation in Unknown Convex Sphere Worlds

Omur Arslan
University of Pennsylvania, omur.arslan@tuebingen.mpg.de

Daniel E. Koditschek
University of Pennsylvania, kod@seas.upenn.edu

Follow this and additional works at: https://repository.upenn.edu/ese_papers

 Part of the Electrical and Computer Engineering Commons, and the Systems Engineering Commons

Recommended Citation
Omur Arslan and Daniel E. Koditschek, "Sensor-Based Reactive Navigation in Unknown Convex Sphere Worlds", . July 2016.

Note: This paper was nominated for the Best Paper Award at the 12th International Workshop on the Algorithmic Foundations of Robotics in 2016.

This paper is posted at ScholarlyCommons. https://repository.upenn.edu/ese_papers/840
For more information, please contact repository@pobox.upenn.edu.

Sensor-Based Reactive Navigation in Unknown Convex Sphere Worlds

Abstract
We construct a sensor-based feedback law that provably solves the real-time collision-free robot navigation problem in a compact convex Euclidean subset cluttered with unknown but sufficiently separated and strongly convex obstacles. Our algorithm introduces a novel use of separating hyperplanes for identifying the robot's local obstacle-free convex neighborhood, affording a reactive (online-computed) piecewise smooth and continuous closed-loop vector field whose smooth flow brings almost all configurations in the robot's free space to a designated goal location, with the guarantee of no collisions along the way. We further extend these provable properties to practically motivated limited range sensing models.

Disciplines
Electrical and Computer Engineering | Engineering | Systems Engineering

Comments
Note: This paper was nominated for the Best Paper Award at the 12th International Workshop on the Algorithmic Foundations of Robotics in 2016.

This conference paper is available at ScholarlyCommons: https://repository.upenn.edu/ese_papers/840

Sensor-Based Reactive Navigation in Unknown Convex Sphere Worlds

Omur Arslan and Daniel E. Koditschek

University of Pennsylvania, Philadelphia, PA 19103, USA
{omur,kod}@seas.upenn.edu

Abstract. We construct a sensor-based feedback law that provably solves the real-time collision-free robot navigation problem in a compact convex Euclidean subset cluttered with unknown but sufficiently separated and strongly convex obstacles. Our algorithm introduces a novel use of separating hyperplanes for identifying the robot's local obstacle-free convex neighborhood, affording a reactive (online-computed) piecewise smooth and continuous closed-loop vector field whose smooth flow brings almost all configurations in the robot's free space to a designated goal location, with the guarantee of no collisions along the way. We further extend these provable properties to practically motivated limited range sensing models.

Keywords: motion planning · collision avoidance · sensor-based planning

1 Introduction

Agile navigation in dense human crowds [1,2], or in natural forests, such as now negotiated by rapid flying [3,4] and legged [5,6] robots, strongly motivates the development of sensor-based reactive motion planners. By the term *reactive* [7, 8] we mean that motion is generated by a vector field arising from some closed-loop feedback policy issuing online force or velocity commands in real time as a function of instantaneous robot state. By the term *sensor-based* we mean that information about the location of the environmental clutter to be avoided is limited to structure perceived within some local neighborhood of the robot's instantaneous position — its sensor footprint.

In this paper, we propose a new reactive motion planner taking the form of a feedback law for a first-order (velocity-controlled), perfectly and relatively (to a fixed goal location) sensed and actuated disk robot, that can be computed using only information about the robot's instantaneous position and structure within its sensor footprint. We assume the a priori unknown environment is a static topological sphere world [9], whose obstacles are convex and have smooth boundaries whose curvature is "reasonably" high relative to their mutual separation. Under these assumptions, the proposed vector field planner is guaranteed to bring all but a measure zero set of initial conditions to the desired goal. To the best of our knowledge, this is the first time a sensor-based reactive motion planner has been shown to be provably correct w.r.t. a general class of environments.

1.1 Motivation and Prior Literature on Vector Field Planners

The simple, computationally efficient artificial potential field approach to real-time obstacle avoidance [10] incurs topologically necessary critical points [11], which, in practice, with no further remediation often include (topologically unnecessary) spurious

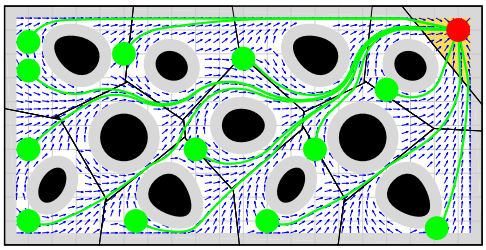

Fig. 1. Exact navigation of a disk-shaped robot using separating hyperplanes of the robot body (red at the goal) and convex obstacles (black solid shapes). Separating hyperplanes between the robot and obstacles define an obstacle-free convex neighborhood (the yellow region when the robot is at the goal) of the robot, and the continuous feedback motion towards the metric projection of a given goal (red) onto this convex set asymptotically steers almost all robot configurations (green) to the goal without collisions along the way. The grey regions represent the augmented workspace boundary and obstacles, and the arrows show the direction of the resulting vector field.

local minima. Even in topologically simple settings such as the sphere worlds addressed here, constructions that eliminate these spurious attractors — e.g., navigation functions [12] — have largely come at the price of complete prior information.

Extensions to navigation functions partially overcoming the necessity of global prior knowledge of (and consequent parameter tuning for) a topologically and metrically simple environment have appeared in the last decade [13, 14]. Sequential composition [15] has been used to cover complicated environments with cellular local potential decompositions [16], but still necessitating prior global knowledge of the environment.

1.2 Contributions and Organization of the Paper

This paper abandons the smooth potential field approach to reactive planning, achieving an algorithm that is "doubly reactive" in the sense that not merely the integrated robot trajectory, but also its generating vector field can be constructed on the fly in real time using only local knowledge of the environment. Our piecewise smooth vector field combines some of the ideas of sensor-based exploration [17] with those of hybrid reactive control [16]. We use separating hyperplanes of convex bodies [18] to identify an obstacle-free convex neighborhood of a robot configuration, and build our safe robot navigation field by control action towards the metric projection of the designated point destination onto this convex set.

Our construction requires no parameter tuning and requires only local knowledge of the environment in the sense that the robot needs only locate those proximal obstacles determining its collision-free convex neighborhood. When the obstacles are sufficiently separated (Assumption 1 stipulates that the robot must be able to pass in between them) and sufficiently strongly convex at their "antipode" (Assumption 2 stipulates that they curve away from the enclosing sphere centered at the destination which just touches their boundary at the most distant point), the proposed vector field generates a smooth flow with a unique attractor at the specified goal along with (the topologically necessary number of) saddles — at least one associated with each obstacle. Since all of its critical points are nondegenerate, our vector field is guaranteed to steer almost all robot configurations to the goal, while avoiding collisions along the way, as illustrated in Fig. 1.

It proves most convenient to develop the theoretical properties of this construction under the assumption that the robot can identify and locate those nearby obstacles whose associated separating hyperplanes define the robot's obstacle-free convex neighborhood (a capability termed *Voronoi-adjacent*[9] *obstacle sensing* in Section 3.2), no matter how physically distant they may be. Thus, to accommodate more physically realistic sensors, we adapt the initial construction (and the proof) to the case of two different limited range sensing modalities, while extending the same formal guarantees as in the erstwhile (local but unbounded range) idealized sensor model.

In prior work [19], we propose a different construction based on power diagrams [20] for navigating among spherical obstacles using knowledge of Voronoi-adjacent[9] obstacles to construct the robot's local workspace [19, Eqn. (9)]. This paper introduces a new construction for that set in (7) based on separating hyperplanes, permitting an extension of the navigable obstacles to the broader class of convex bodies specified by Assumption 2, while providing the same guarantee of almost global asymptotic convergence (Theorem 3) to a given goal location. From the view of applications, the new appeal to separating hyperplanes permits the central advance of a purely reactive construction from limited range sensors (22), e.g., in the planar case from immediate line-of-sight appearance (27), with the same global guarantees.

This paper is organized as follows. Section 2 continues with a formal statement of the problem at hand. Section 3 briefly summarizes a separating hyperplane theorem of convex bodies, and introduces its use for identifying collision-free robot configurations. Section 4, comprising the central contribution of the paper, constructs and analyzes the reactive vector field planner for safe robot navigation in a convex sphere world, and provides its more practical extensions. Section 5 illustrates the qualitative properties of the proposed vector field planner using numerical simulations. Section 6 concludes with a summary of our contributions and a brief discussion of future work.

2 Problem Formulation

Consider a disk-shaped robot, of radius $r \in \mathbb{R}_{>0}$ centered at $\mathrm{x} \in \mathcal{W}$, operating in a closed compact convex environment $\mathcal{W}$ in the n-dimensional Euclidean space $\mathbb{R}^n$, where $n \geq 2$, punctured with $m \in \mathbb{N}$ open convex sets $\mathcal{O} := \{O_1, O_2, \ldots, O_m\}$ with twice differentiable boundaries, representing obstacles.[1] Hence, the free space $\mathcal{F}$ of the robot is given by

$$\mathcal{F} := \Big\{ \mathrm{x} \in \mathcal{W} \Big| \, \overline{B(\mathrm{x}, r)} \subseteq \mathcal{W} \setminus \bigcup\nolimits_{i=1}^{m} O_i \Big\}, \tag{1}$$

where $B(\mathrm{x}, r) := \big\{ \mathrm{q} \in \mathbb{R}^n \big| \|\mathrm{q} - \mathrm{x}\| < r \big\}$ is the open ball centered at x with radius r, and $\overline{B(\mathrm{x}, r)}$ denotes its closure, and $\|.\|$ denotes the standard Euclidean norm.

To maintain the local convexity of obstacle boundaries in the free space $\mathcal{F}$, we assume that our disk-shaped robot can freely fit in between (and thus freely circumnavigate) any of the obstacles throughout the workspace $\mathcal{W}$: [2]

[1] Here, $\mathbb{N}$ is the set of all natural numbers; $\mathbb{R}$ and $\mathbb{R}_{>0}$ ($\mathbb{R}_{\geq 0}$) denote the set of real and positive (nonnegative) real numbers, respectively.

[2] Assumption 1 is equivalent to the "isolated" obstacles assumption of [12].

Assumption 1. *Obstacles are separated from each other by clearance of at least* $d(O_i, O_j) > 2r$ *for all* $i \neq j$*, and from the boundary* $\partial\mathcal{W}$ *of the workspace* $\mathcal{W}$ *as* $d(O_i, \partial\mathcal{W}) > 2r$ *for all* $i = 1 \dots m$*, where* $d(A, B) := \inf\{\|\mathrm{a} - \mathrm{b}\| \,|\, \mathrm{a} \in A, \mathrm{b} \in B\}$.

Before formally stating our navigation problem, it is useful to recall a known topological limitation of reactive planners: if a continuous vector field planner on a generalized sphere world has a unique attractor, then it must have at least as many saddles as obstacles [9]. In consequence, the robot navigation problem that we seek to solve is:

Reactive Navigation Problem. *Assuming the first-order (completely actuated single-integrator) robot dynamics,*

$$\dot{\mathrm{x}} = \mathrm{u}(\mathrm{x}) \,, \tag{2}$$

find a Lipschitz continuous vector field controller, $\mathrm{u} : \mathcal{F} \to \mathbb{R}^n$*, that leaves the robot's free space* $\mathcal{F}$ *positively invariant and asymptotically steers almost all robot configurations in* $\mathcal{F}$ *to any given goal location* $\mathrm{x}^* \in \mathcal{F}$.

3 Encoding Collisions via Separating Hyperplanes

3.1 Separating Hyperplane Theorem

A fundamental theorem of convex sets states that any two nonintersecting convex sets can be separated by a hyperplane such that they lie on opposite sides of this hyperplane:

Theorem 1 ([18, 21]). *For any two disjoint convex sets* $A, B \in \mathbb{R}^n$ *(i.e.,* $A \cap B = \varnothing$*), there exists* $\mathrm{a} \in \mathbb{R}^n$ *and* $b \in \mathbb{R}$ *such that* $\mathrm{a}^{\mathrm{T}}\mathrm{x} \geq b$ *for all* $\mathrm{x} \in A$ *and* $\mathrm{a}^{\mathrm{T}}\mathrm{x} \leq b$ *for all* $\mathrm{x} \in B$.

For example, a usual choice of such a hyperplane is [18]:

Definition 1. *The* maximum margin separating hyperplane *of any two disjoint convex sets* $A, B \subset \mathbb{R}^n$*, with* $d(A, B) > 0$*, is defined to be*

$$H(A, B) := \left\{ \mathrm{x} \in \mathbb{R}^n \,\middle|\, \|\mathrm{x} - \mathrm{a}\| = \|\mathrm{x} - \mathrm{b}\|, \|\mathrm{a} - \mathrm{b}\| = d(A, B), \mathrm{a} \in \overline{A}, \mathrm{b} \in \overline{B} \right\} , \tag{3}$$

where $d(\mathrm{x}, H(A, B)) \geq \frac{d(A,B)}{2}$ *for all* $\mathrm{x} \in A \cup B$.

Another useful tool for finding separating hyperplanes is metric projection:

Theorem 2 ([21]). *Let* $A \subset \mathbb{R}^n$ *be a closed convex set and* $\mathrm{x} \in \mathbb{R}^n$*. Then there exists a unique point* $\mathrm{a}^* \in A$ *such that*

$$\mathrm{a}^* = \Pi_A(\mathrm{x}) := \underset{\mathrm{a} \in A}{\arg\min} \|\mathrm{a} - \mathrm{x}\|, \tag{4}$$

and one has $(\mathrm{x} - \Pi_A(\mathrm{x}))^{\mathrm{T}}(\Pi_A(\mathrm{x}) - \mathrm{a}) \geq 0$ *for all* $\mathrm{a} \in A$.

The map $\Pi_A(\mathrm{x})$ *is called the* metric projection *of* x *onto set* A .

Lemma 1. *The maximum margin separating hyperplane of a convex set* $A \subset \mathbb{R}^n$ *and the ball* $B(\mathrm{x}, r)$ *of radius* $r \in \mathbb{R}_{>0}$ *centered at* $\mathrm{x} \in \mathbb{R}^n$*, satisfying* $d(\mathrm{x}, A) \geq r$*, is given by*

$$H(A, B(\mathrm{x}, r)) = \left\{ \mathrm{y} \in \mathbb{R}^n \,\middle|\, \left\| \mathrm{y} - (\Pi_{\overline{B(\mathrm{x},r)}} \circ \Pi_{\overline{A}})(\mathrm{x}) \right\| = \|\mathrm{y} - \Pi_{\overline{A}}(\mathrm{x})\| \right\} , \tag{5}$$

where $(\Pi_{\overline{B(\mathrm{x},r)}} \circ \Pi_{\overline{A}})(\mathrm{x}) = \mathrm{x} - r\frac{\mathrm{x} - \Pi_{\overline{A}}(\mathrm{x})}{\|\mathrm{x} - \Pi_{\overline{A}}(\mathrm{x})\|}$.

Proof. See Appendix I-A in Supplementary Material. ■

A common application of separating hyperplanes of a set of convex bodies is to discover their organizational structure. For instance, to model its topological structure, we define the generalized Voronoi diagrams $\mathcal{V} = \{V_1, V_2, \ldots, V_m\}$ of a convex environment $\mathcal{W}$ in $\mathbb{R}^n$ populated with disjoint convex obstacles $\mathcal{O} = \{O_1, O_2, \ldots, O_m\}$ (i.e., $d(O_i, O_j) > 0$ for all $i \neq j$), based on maximum margin separating hyperplanes, to be[3] [4]

$$V_i := \Big\{ \mathrm{q} \in \mathcal{W} \Big| \|\mathrm{q}-\mathrm{p}_i\| \leq \|\mathrm{q}-\mathrm{p}_j\|, \|\mathrm{p}_i-\mathrm{p}_j\| = d(O_i, O_j), \mathrm{p}_i \in \overline{O}_i, \mathrm{p}_j \in \overline{O}_j \quad \forall j \neq i \Big\}, \tag{6}$$

which yields a convex cell decomposition of a subset of $\mathcal{W}$ such that, by construction, each obstacle is contained in its Voronoi cell, i.e., $O_i \subset V_i$, see Fig. 2. Note that for point obstacles, say $O_i = \{\mathrm{p}_i\}$ for some $\mathrm{p}_i \in \mathbb{R}^n$, the generalized Voronoi diagram of $\mathcal{W}$ in (6) simplifies back to the standard Voronoi diagram of $\mathcal{W}$, generated by points $\{\mathrm{p}_1, \ldots, \mathrm{p}_m\}$, i.e., $V_i = \big\{ \mathrm{q} \in \mathcal{W} \big| \|\mathrm{q}-\mathrm{p}_i\| \leq \|\mathrm{q}-\mathrm{p}_j\|, \ \forall j \neq i \big\}$ [27].

3.2 The Safe Neighborhood of a Disk-Shaped Robot

Throughout the sequel, we consider a disk-shaped robot, centered at $\mathrm{x} \in \mathcal{W}$ with radius $r \in \mathbb{R}_{>0}$, moving in a closed compact convex environment $\mathcal{W} \subseteq \mathbb{R}^n$ populated with open convex obstacles, $\mathcal{O} = \{O_1, O_2, \ldots, O_m\}$, satisfying Assumption 1. Since the workspace, obstacles, and the robot radius are fixed, we suppress all mention of the associated terms wherever convenient, in order to simplify the notation.

Using the robot body and obstacles as generators of a generalized Voronoi diagram of $\mathcal{W}$, we define the robot's *local workspace*, $\mathcal{LW}(\mathrm{x})$, illustrated in Fig. 2(left), as,[5]

$$\mathcal{LW}(\mathrm{x}) := \left\{ \mathrm{q} \in \mathcal{W} \left| \left\| \mathrm{q} - \mathrm{x} + r \frac{\mathrm{x} - \Pi_{\overline{O}_i}(\mathrm{x})}{\left\| \mathrm{x} - \Pi_{\overline{O}_i}(\mathrm{x}) \right\|} \right\| \leq \left\| \mathrm{q} - \Pi_{\overline{O}_i}(\mathrm{x}) \right\|, \quad \forall i \right\}. \tag{7}$$

Note that we here take the advantage of having a disk-shaped robot and construct the maximum margin separating hyperplane between the robot and each obstacle using the robot's centroid (Lemma 1).

A critical property of the local workspace $\mathcal{LW}$ is:

Proposition 1. *A robot placement* $\mathrm{x} \in \mathcal{W} \setminus \bigcup_{i=1}^m O_i$ *is collision free, i.e.,* $\mathrm{x} \in \mathcal{F}$*, if and only if the robot body is contained in its local workspace* $\mathcal{LW}(\mathrm{x})$*, i.e.,* [6]

$$\mathrm{x} \in \mathcal{F} \iff \overline{B(\mathrm{x}, r)} \subseteq \mathcal{LW}(\mathrm{x}) \,. \tag{8}$$

Proof. See Supplementary Material Appendix I-B. ■

[3] Generalized Voronoi diagrams and cell decomposition methods are traditionally encountered in the design of roadmap methods [8,17,22]. A major distinction between our construction and these roadmap algorithms is that the latter typically seek a global, one-dimensional graphical representation of a robot's environment (independent of any specific configuration), whereas our approach uses the local open interior cells of the robot-centric Voronoi diagram to determine a locally safe neighborhood of a given free configuration.

[4] It seems worth noting that our use of generalized Voronoi diagrams is motivated by application of Voronoi diagrams in robotics for coverage control of distributed sensor networks [23–26].

[5] Here, to solve the indeterminacy, we set $\frac{\mathrm{x}}{\|\mathrm{x}\|} = 0$ whenever $\mathrm{x} = 0$.

[6] Note that $\mathcal{F} \subsetneq \mathcal{W} \setminus \bigcup_{i=1}^m O_i$ for a disk-shaped robot of radius $r > 0$.

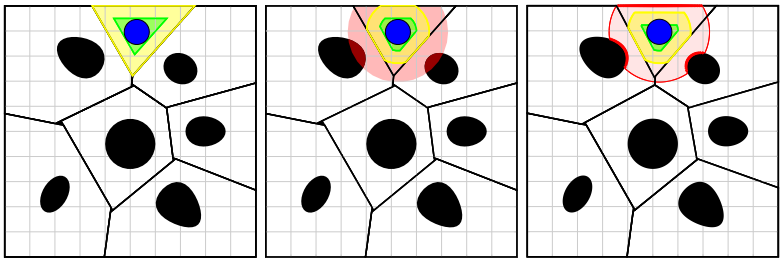

Fig. 2. Local workspace $\mathcal{LW}$ (yellow) and local free space $\mathcal{LF}$ (green) of a disk-shaped robot (blue) for different sensing modalities: (left) Voronoi-adjacent[9] obstacle sensing, (middle) a fixed radius sensory footprint (red), (right) a limited range line-of-sight sensor (red). The boundary of each generalized Voronoi cell is defined by the maximum margin separating hyperplanes of the robot body (blue) and obstacles (black).

Accordingly, we define the robot's *local free space*, $\mathcal{LF}(\mathrm{x})$, by eroding $\mathcal{LW}(\mathrm{x})$, removing the volume swept along its boundary, $\partial\mathcal{LW}(\mathrm{x})$, by the robot body radius, illustrated on the left in Fig. 2, as [28] [7]

$$\mathcal{LF}(\mathrm{x}) := \mathcal{LW}(\mathrm{x}) \setminus \big(\partial\mathcal{LW}(\mathrm{x}) \oplus B(\mathbf{0}, r)\big) = \Big\{ \mathrm{q} \in \mathcal{LW}(\mathrm{x}) \Big| \overline{B(\mathrm{q}, r)} \subseteq \mathcal{LW}(\mathrm{x}) \Big\} \,. \quad (9)$$

Note that, for any $\mathrm{x} \in \mathcal{F}$, $\mathcal{LF}(\mathrm{x})$ is a nonempty closed convex set, because $\mathrm{x} \in \mathcal{LF}(\mathrm{x})$ and the erosion of a closed convex set by an open ball is a closed convex set.[8]

An immediate consequence of Proposition 1 is:

Corollary 1. *Any robot placement in the local free space $\mathcal{LF}(\mathrm{x})$ of a collision free robot location $\mathrm{x} \in \mathcal{F}$ is also collision free, i.e., $\mathcal{LF}(\mathrm{x}) \subseteq \mathcal{F}$ for all $\mathrm{x} \in \mathcal{F}$.*

Finally, it is useful to emphasize that to construct its local workspace, the robot requires only local knowledge of the environment in the sense that the robot only needs to locate proximal obstacles — those whose Voronoi cells are adjacent[9] to the robot's (local workspace). This can be achieved by assuming an adjustable radius sensory footprint and gradually increasing its sensing range until the set of obstacles in the sensing range satisfies a certain geometric criterion guaranteeing that the detected obstacles exactly define the robot's local workspace [23]. We will refer to this sensing model as *Voronoi-adjacent obstacle sensing*.

4 Robot Navigation via Separating Hyperplanes

In this section, first assuming Voronoi-adjacent obstacle sensing, we introduce a new provably correct vector field controller for safe robot navigation in a convex sphere world, and list its important qualitative properties. Then we present its extensions for two more realistic sensor models (illustrated, respectively, in the middle and the right panels of Fig. 2): a fixed radius sensory footprint and a limited range line-of-sight sensor.

[7] Here, $\mathbf{0}$ is a vector of all zeros with the appropriate size, and $A \oplus B$ denotes the Minkowski sum of sets A and B defined as $A \oplus B = \{a + b \mid a \in A, b \in B\}$.

[8] The erosion of a closed half-space by an open ball is a closed half-space, and a closed convex set can be defined as (possibly infinite) intersection of closed half-spaces [18]. Thus, since the erosion operation is distributed over set intersection [28], and an arbitrary intersection of closed sets is closed [29], the erosion of a closed convex set by an open ball is a closed convex set.

[9] A pair of Voronoi cells in $\mathbb{R}^n$ is said to be *adjacent* if they share a $n-1$ dimensional face.

4.1 Feedback Robot Motion Planner

Assuming the fully-actuated single-integrator robot dynamics in (2), for a choice of a desired goal location $\mathrm{x}^* \in \mathcal{F}$, we propose a robot navigation strategy, called the "*move-to-projected-goal*" law, $\mathrm{u} : \mathcal{F} \to \mathbb{R}^n$ that steers the robot at location $\mathrm{x} \in \mathcal{F}$ towards the global goal x^* through the "*projected goal*", $\Pi_{\mathcal{LF}(\mathrm{x})}(\mathrm{x}^*)$, as follows: [10]

$$\mathrm{u}(\mathrm{x}) = -k\big(\mathrm{x} - \Pi_{\mathcal{LF}(\mathrm{x})}(\mathrm{x}^*)\big) \,, \tag{10}$$

where $k \in \mathbb{R}_{>0}$ is a fixed control gain and Π_A (4) is the metric projection onto a closed convex set $A \subset \mathbb{R}^n$, and $\mathcal{LF}(\mathrm{x})$ is continuously updated using the Voronoi-adjacent obstacle sensing and its relation with $\mathcal{LW}(\mathrm{x})$ in (9).

4.2 Qualitative Properties

Proposition 2. *The "move-to-projected-goal" law in (10) is piecewise continuously differentiable.*

Proof. An important property of generalized Voronoi diagrams in (6) inherited from the standard Voronoi diagrams of point generators is that the boundary of each Voronoi cell is a piecewise continuously differentiable function of generator locations [31, 32]. In particular, for any $\mathrm{x} \in \mathcal{F}$, the boundary of the robot's local workspace $\mathcal{LW}(\mathrm{x})$ is piecewise continuously differentiable since it is defined by the boundary of the workspace and separating hyperplanes between the robot and obstacles, parametrized by x and $\Pi_{\overline{O}_i}(\mathrm{x})$, and metric projections onto convex cells are piecewise continuously differentiable [33]. Hence, the boundary of the local free space $\mathcal{LF}(\mathrm{x})$ is also piecewise continuously differentiable, because $\mathcal{LF}(\mathrm{x})$ is the nonempty erosion of $\mathcal{LW}(\mathrm{x})$ by a fixed open ball. Therefore, one can conclude using the sensitivity analysis of metric projections onto moving convex sets [34, 35] that the "move-to-projected-goal" law is Lipschitz continuous and piecewise continuously differentiable. ■

Proposition 3. *The robot's free space $\mathcal{F}$ in (1) is positively invariant under the "move-to-projected" law (10).*

Proof. Since x and $\Pi_{\mathcal{LF}(\mathrm{x})}(\mathrm{x}^*)$ are both in $\mathcal{LF}(\mathrm{x})$ for any $\mathrm{x} \in \mathcal{F}$, and $\mathcal{LF}(\mathrm{x})$ is an obstacle free convex neighborhood of x (Corollary 1), the line segment joining x and $\Pi_{\mathcal{LF}(\mathrm{x})}(\mathrm{x}^*)$ is free of collisions. Hence, at the boundary of $\mathcal{F}$, the robot under the "move-to-projected-goal" law either stays on the boundary or moves towards the interior of $\mathcal{F}$, but never crosses the boundary, and so the result follows. ■

Proposition 4. *For any initial $\mathrm{x} \in \mathcal{F}$, the "move-to-projected-goal" law (10) has a unique continuously differentiable flow in $\mathcal{F}$ (1) defined for all future time.*

[10] In general, the metric projection of a point onto a convex set can be efficiently computed using an off-the-shelf convex programming solver [18]. If $\mathcal{W}$ is a convex polytope, then the robot's local free space $\mathcal{LF}(\mathrm{x})$ is also a convex polytope and can be written as a finite intersection of half-spaces. Thus, the metric projection onto a convex polytope can be recast as quadratic programming and can be solved in polynomial time [30]. In the case of a convex polygonal environment, $\mathcal{LF}(\mathrm{x})$ is a convex polygon and the metric projection onto it can be solved analytically since the solution lies on one of its edges, unless the input point is inside $\mathcal{LF}(\mathrm{x})$.

Proof. The existence, uniqueness and continuous differentiability of its flow follow from the Lipschitz continuity of the "move-to-projected-goal" law in its compact domain $\mathcal{F}$, because a piecewise continuously differentiable function is locally Lipschitz on its domain [36], and a locally Lipschitz function on a compact set is globally Lipschitz on that set [37]. ■

Proposition 5. *The set of stationary points of the "move-to-projected-goal" law (10) is* $\{\mathrm{x}^*\} \cup \bigcup_{i=1}^{m} \mathfrak{S}_i$*, where*

$$\mathfrak{S}_i := \left\{ \mathrm{x} \in \mathcal{F} \,\middle|\, d(\mathrm{x}, O_i) = r,\ \frac{(\mathrm{x}-\Pi_{\overline{O}_i}(\mathrm{x}))^{\mathrm{T}}(\mathrm{x}-\mathrm{x}^*)}{\|\mathrm{x}-\Pi_{\overline{O}_i}(\mathrm{x})\|\|\mathrm{x}-\mathrm{x}^*\|} = 1 \right\} . \tag{11}$$

Proof. It follows from (4) and $\mathrm{x}^* \in \mathcal{LF}(\mathrm{x}^*)$ that the goal x^* is a stationary point of (10). In fact, for any $\mathrm{x} \in \mathcal{F}$, one has $\Pi_{\mathcal{LF}(\mathrm{x})}(\mathrm{x}^*) = \mathrm{x}^*$ whenever $\mathrm{x}^* \in \mathcal{LF}(\mathrm{x})$. Hence, in the sequel of the proof, we only consider the set of robot locations satisfying $\mathrm{x}^* \notin \mathcal{LF}(\mathrm{x})$.

Let $\mathrm{x} \in \mathcal{F}$ such that $\mathrm{x}^* \notin \mathcal{LF}(\mathrm{x})$. Recall from (7) and (9) that $\mathcal{LW}(\mathrm{x})$ is determined by the maximum margin separating hyperplanes of the robot body and obstacles, and $\mathcal{LF}(\mathrm{x})$ is obtained by eroding $\mathcal{LW}(\mathrm{x})$ by an open ball of radius r. Hence, x lies in the interior of $\mathcal{LF}(\mathrm{x})$ if and only if $d(\mathrm{x}, O_i) > r$ for all i. As a result, since $\mathrm{x}^* \notin \mathcal{LF}(\mathrm{x})$, one has $\mathrm{x} = \Pi_{\mathcal{LF}(\mathrm{x})}(\mathrm{x}^*)$ only if $d(\mathrm{x}, O_i) = r$ for some i.

Note that if $d(\mathrm{x}, O_i) = r$, then, since $d(O_i, O_j) > 2r$ (Assumption 1), $d(\mathrm{x}, O_j) > r$ for all $j \neq i$. Therefore, there can be only one obstacle index i such that $\mathrm{x} = \Pi_{\mathcal{LW}(\mathrm{x})}(\mathrm{x}^*)$ and $d(\mathrm{x}, O_i) = r$. Further, given $d(\mathrm{x}, O_i) = r$, since $\Pi_{\mathcal{LF}(\mathrm{x})}(\mathrm{x}^*)$ is the unique closest point of the closed convex set $\mathcal{LF}(\mathrm{x})$ to the goal x^* (Theorem 2), its optimality [18] implies that one has $\mathrm{x} = \Pi_{\mathcal{LW}(\mathrm{x})}(\mathrm{x}^*)$ if and only if the maximum margin separating hyperplane between the robot and obstacle O_i is tangent to the level curve of the squared Euclidean distance to the goal, $\|\mathrm{x} - \mathrm{x}^*\|^2$, at $\Pi_{\overline{O}_i}(\mathrm{x})$, and separates x and x^*, i.e.,

$$\frac{(\mathrm{x} - \Pi_{\overline{O}_i}(\mathrm{x}))^{\mathrm{T}}(\mathrm{x} - \mathrm{x}^*)}{\|\mathrm{x} - \Pi_{\overline{O}_i}(\mathrm{x})\|\|\mathrm{x} - \mathrm{x}^*\|} = 1. \tag{12}$$

Thus, one can locate the stationary points of the "move-to-projected-goal" law in (10) associated with obstacle O_i as in (11), and so the result follows. ■

Note that, for any equilibrium point $\mathrm{s}_i \in \mathfrak{S}_i$ associated with obstacle O_i, one has that the equilibrium s_i, its projection $\Pi_{\overline{O}_i}(\mathrm{s}_i)$ and the goal x^* are all collinear.

Lemma 2. *The "move-to-projected-goal" law (10) in a small neighborhood of the goal* x^* *is given by*

$$\mathrm{u}(\mathrm{x}) = -k(\mathrm{x} - \mathrm{x}^*), \quad \forall\, \mathrm{x} \in B(\mathrm{x}^*, \epsilon)\ , \tag{13}$$

for some $\epsilon > 0$*; and around any stationary point* $\mathrm{s}_i \in \mathfrak{S}_i$ *(11), associated with obstacle* O_i*, it is given by*

$$\mathrm{u}(\mathrm{x}) = -k\left(\mathrm{x} - \mathrm{x}^* + \frac{\big(\mathrm{x} - \Pi_{\overline{O}_i}(\mathrm{x})\big)^{\mathrm{T}}(\mathrm{x}^* - \mathrm{h}_i)}{\big\|\mathrm{x} - \Pi_{\overline{O}_i}(\mathrm{x})\big\|^2}\big(\mathrm{x} - \Pi_{\overline{O}_i}(\mathrm{x})\big)\right), \tag{14}$$

for all $\mathrm{x} \in B(\mathrm{s}_i, \varepsilon)$ *and some* $\varepsilon > 0$*, where*

$$\mathrm{h}_i := \frac{\mathrm{x} + \Pi_{\overline{O}_i}(\mathrm{x})}{2} + \frac{r}{2}\frac{\mathrm{x} - \Pi_{\overline{O}_i}(\mathrm{x})}{\big\|\mathrm{x} - \Pi_{\overline{O}_i}(\mathrm{x})\big\|}\ . \tag{15}$$

Proof. See Supplementary Material Appendix I-C. ■

Since our "move-to-projected-goal" law strictly decreases the Euclidean distance to the goal x^* away from its stationary points (Proposition 7), to guarantee the existence of a unique stable attractor at x^*, we require the following assumption[11], whose geometric interpretation is discussed in detail in Appendix II in Supplementary Material.

Assumption 2. *(Curvature Condition) The Jacobian matrix* $\mathbf{J}_{\Pi_{\overline{O}_i}}(\mathrm{s}_i)$ *of the metric projection of any stationary point* $\mathrm{s}_i \in \mathfrak{S}_i$ *onto the associated obstacle* O_i *satisfies*[12]

$$\mathbf{J}_{\Pi_{\overline{O}_i}}(\mathrm{s}_i) \prec \frac{\left\|\mathrm{x}^* - \Pi_{\overline{O}_i}(\mathrm{s}_i)\right\|}{r + \left\|\mathrm{x}^* - \Pi_{\overline{O}_i}(\mathrm{s}_i)\right\|}\mathbf{I} \qquad \forall i, \tag{16}$$

where $\mathbf{I}$ *is the identity matrix of appropriate size.*

Proposition 6. *If Assumption 2 holds for the goal* x^* *and for all obstacles, then* x^* *is the only locally stable equilibrium of the "move-to-projected-goal" law (10), and all stationary points,* $\mathrm{s}_i \in \mathfrak{S}_i$ *(11), associated with obstacles,* O_i*, are nondegenerate saddles.*

Proof. It follows from (13) that the goal x^* is a locally stable point of the "move-to-projected-goal" law, because its Jacobian matrix, $\mathbf{J}_{\mathrm{u}}(\mathrm{x}^*)$, at x^* is equal to $-k\,\mathbf{I}$.

To determine the type of any stationary point $\mathrm{s}_i \in \mathfrak{S}_i$ associated with obstacle O_i, define

$$g(\mathrm{x}) := \frac{\big(\mathrm{x}^* - \Pi_{\overline{O}_i}(\mathrm{x})\big)^{\mathrm{T}}\big(\mathrm{x} - \Pi_{\overline{O}_i}(\mathrm{x})\big)}{\big\|\mathrm{x} - \Pi_{\overline{O}_i}(\mathrm{x})\big\|^2} - \frac{r}{2\big\|\mathrm{x} - \Pi_{\overline{O}_i}(\mathrm{x})\big\|} - \frac{1}{2}\,, \tag{17}$$

and so the "move-to-projected-goal" law in a small neighborhood of s_i in (14) can be rewritten as

$$\mathrm{u}(\mathrm{x}) = -k\Big(\mathrm{x} - \mathrm{x}^* + g(\mathrm{x})\big(\mathrm{x} - \Pi_{\overline{O}_i}(\mathrm{x})\big)\Big)\,. \tag{18}$$

Hence, using $\left\|\mathrm{s}_i - \Pi_{\overline{O}_i}(\mathrm{s}_i)\right\| = r$, one can verify that its Jacobian matrix at s_i is given by

$$\mathbf{J}_{\mathrm{u}}(\mathrm{s}_i) = -kg(\mathrm{s}_i)\left(\frac{\left\|\mathrm{x}^* - \Pi_{\overline{O}_i}(\mathrm{s}_i)\right\|}{r + \left\|\mathrm{x}^* - \Pi_{\overline{O}_i}(\mathrm{s}_i)\right\|}\mathbf{Q} - \mathbf{J}_{\Pi_{\overline{O}_i}}(\mathrm{s}_i)\right) - \tfrac{k}{2}(\mathbf{I} - \mathbf{Q})\,, \tag{19}$$

where $g(\mathrm{s}_i) = -\dfrac{\left\|\mathrm{x}^* - \Pi_{\overline{O}_i}(\mathrm{s}_i)\right\|}{r} - 1 < -2$, and

$$\mathbf{Q} = \mathbf{I} - \frac{\big(\mathrm{s}_i - \Pi_{\overline{O}_i}(\mathrm{s}_i)\big)\big(\mathrm{s}_i - \Pi_{\overline{O}_i}(\mathrm{s}_i)\big)^{\mathrm{T}}}{\big\|\mathrm{s}_i - \Pi_{\overline{O}_i}(\mathrm{s}_i)\big\|^2}. \tag{20}$$

Note that $\mathbf{J}_{\Pi_{\overline{O}_i}}(\mathrm{x})\big(\mathrm{x} - \Pi_{\overline{O}_i}(\mathrm{x})\big) = 0$ for all $\mathrm{x} \in \mathbb{R}^n \setminus \overline{O}_i$ [39, 40]. Hence, if Assumption 2 holds, then one can conclude from $g(\mathrm{s}_i) < -2$ and (19) that the only negative eigenvalue of $\mathbf{J}_{\mathrm{u}}(\mathrm{s}_i)$ and the associated eigenvector are $-\frac{k}{2}$ and $\big(\mathrm{s}_i - \Pi_{\overline{O}_i}(\mathrm{s}_i)\big)$, respectively; and all other eigenvalues of $\mathbf{J}_{\mathrm{u}}(\mathrm{s}_i)$ are positive. Thus, s_i is a nondegenerate saddle point of the "move-to-projected-goal" law associated with O_i. ■

[11] A similar obstacle curvature condition is necessarily made in the design of navigation functions for spaces with convex obstacles in [38].

[12] For any two symmetric matrices $\mathbf{A}, \mathbf{B} \in \mathbb{R}^{N\times N}$, $\mathbf{A} \prec \mathbf{B}$ (and $\mathbf{A} \preccurlyeq \mathbf{B}$) means that $\mathbf{B} - \mathbf{A}$ is positive definite (positive semidefinite, respectively).

Proposition 7. *Given that the goal location* x^* *and all obstacles satisfy Assumption 2, the goal* x^* *is an asymptotically stable equilibrium of the "move-to-projected-goal" law (10), whose basin of attraction includes* $\mathcal{F}$*, except a set of measure zero.*

Proof. Consider the squared Euclidean distance to the goal as a smooth Lyapunov function candidate, i.e., $V(\mathrm{x}) := \|\mathrm{x} - \mathrm{x}^*\|^2$, and it follows from (4) and (10) that

$$\dot{V}(\mathrm{x}) = -k \underbrace{2(\mathrm{x} - \mathrm{x}^*)^{\mathrm{T}} \big(\mathrm{x} - \Pi_{\mathcal{L}\mathcal{F}(\mathrm{x})}(\mathrm{x}^*)\big)}_{\substack{\geq \left\|\mathrm{x} - \Pi_{\mathcal{L}\mathcal{F}(\mathrm{x})}(\mathrm{x}^*)\right\|^2 \\ \text{since } \mathrm{x} \in \mathcal{L}\mathcal{F}(\mathrm{x}) \text{ and } \|\mathrm{x}-\mathrm{x}^*\|^2 \geq \left\|\Pi_{\mathcal{L}\mathcal{F}(\mathrm{x})}(\mathrm{x}^*) - \mathrm{x}^*\right\|^2}} \leq -k \left\|\mathrm{x} - \Pi_{\mathcal{L}\mathcal{F}(\mathrm{x})}(\mathrm{x}^*)\right\|^2 \leq 0 \,, \tag{21}$$

which is zero iff x is a stationary point. Hence, we have from LaSalle's Invariance Principle [37] that all robot configurations in $\mathcal{F}$ asymptotically reach the set of equilibria of (10). Therefore, the result follows from Proposition 2 and Proposition 6, because, under Assumption 2, x^* is the only stable stationary point of the piecewise continuous "move-to-projected-goal" law (10), and all other stationary points are nondegenerate saddles whose stable manifolds have empty interiors [41]. ■

Finally, we find it useful to summarize important qualitative properties of the "move-to-projected-goal" law as:

Theorem 3. *The piecewise continuously differentiable "move-to-projected-goal" law in (10) leaves the robot's free space* $\mathcal{F}$ *(1) positively invariant; and if Assumption 2 holds, then its unique continuously differentiable flow, starting at almost any configuration* $\mathrm{x} \in \mathcal{F}$*, asymptotically reaches the goal location* x^**, while strictly decreasing the squared Euclidean distance to the goal,* $\|\mathrm{x} - \mathrm{x}^*\|^2$*, along the way.*

4.3 Extensions for Limited Range Sensing Modalities

Navigation using a Fixed Radius Sensory Footprint. A crucial property of the "move-to-projected-goal" law (10) is that it only requires the knowledge of the robot's Voronoi-adjacent[9] obstacles to determine the robot's local workspace and so the robot's local free space. We now exploit that property to relax our construction so that it can be put to practical use with commonly available sensors that have bounded radius footprint.[13] We will present two specific instances, pointing out along the way how they nevertheless preserve the sufficient conditions for the qualitative properties listed in Section 4.2.

Suppose the robot is equipped with a sensor with a fixed sensing range, $R \in \mathbb{R}_{>0}$, whose sensory output, denoted by $\mathcal{S}_R(\mathrm{x}) := \{S_1, S_2, \ldots, S_m\}$, at a location, $\mathrm{x} \in \mathcal{W}$, returns some computationally effective dense representation of the perceptible portion, $S_i := O_i \cap B(\mathrm{x}, R)$, of each obstacle, O_i, in its sensory footprint, $B(\mathrm{x}, R)$. Note that S_i is always open and might possibly be empty (if O_i is outside the robot's sensing range), see Fig. 2(middle); and we assume that the robot's sensing range is greater than the robot body radius, i.e., $R > r$.

[13] This extension results from the construction of the robot's local workspace (7) in terms of the maximum margin separating hyperplanes of convex sets. In consequence, because the intersection of convex sets is a convex set [18], perceived obstacles in the robot's (convex) sensory footprint are, in turn, themselves always convex.

As in (7), using the maximum margin separating hyperplanes of the robot and sensed obstacles, we define the robot's *sensed local workspace*, see Fig. 2(middle), as,

$$\mathcal{LW}_{\mathbb{S}}(\mathrm{x}) := \Big\{ \mathrm{q} \in \mathcal{W} \cap \overline{B\big(\mathrm{x}, \tfrac{r+R}{2}\big)} \,\Big|\, \Big\| \mathrm{q} - \mathrm{x} + r \tfrac{\mathrm{x} - \Pi_{\overline{S}_i}(\mathrm{x})}{\|\mathrm{x} - \Pi_{\overline{S}_i}(\mathrm{x})\|} \Big\| \leq \big\| \mathrm{q} - \Pi_{\overline{S}_i}(\mathrm{x}) \big\|, \forall i \text{ s.t. } S_i \neq \varnothing \Big\}. \quad (22)$$

Note that $\overline{B\big(\mathrm{x}, \frac{r+R}{2}\big)}$ is equal to the intersection of the closed half spaces containing the robot body and defined by the maximum margin separating hyperplanes of the robot body, $\overline{B(\mathrm{x}, r)}$, and all individual points, $\mathrm{q} \in \mathbb{R}^n \setminus B(\mathrm{x}, R)$, outside its sensory footprint.

An important observation revealing a critical connection between the robot's local workspace $\mathcal{LW}$ in (7) and its sensed local workspace $\mathcal{LW}_{\mathbb{S}}$ in (22) is:

Proposition 8. *$\mathcal{LW}_{\mathbb{S}}(\mathrm{x}) = \mathcal{LW}(\mathrm{x}) \cap \overline{B\big(\mathrm{x}, \frac{r+R}{2}\big)}$ for all $\mathrm{x} \in \mathcal{W}$.*

Proof. See Appendix I-D in Supplementary Material. ■

In accordance with its local free space $\mathcal{LF}(\mathrm{x})$ in (9), we define the robot's *sensed local free space* $\mathcal{LF}_{\mathbb{S}}(\mathrm{x})$ by eroding $\mathcal{LW}_{\mathbb{S}}(\mathrm{x})$ by the robot body, illustrated in Fig. 2(middle), as,

$$\mathcal{LF}_{\mathbb{S}}(\mathrm{x}) := \Big\{ \mathrm{q} \in \mathcal{LW}_{\mathbb{S}}(\mathrm{x}) \,\Big|\, \overline{B(\mathrm{q}, r)} \subseteq \mathcal{LW}_{\mathbb{S}}(\mathrm{x}) \Big\} = \mathcal{LF}(\mathrm{x}) \cap \overline{B\big(\mathrm{x}, \tfrac{R-r}{2}\big)}\,, \quad (23)$$

where the latter follows from Proposition 8 and that the erosion operation is distributed over set intersection [28]. Note that, for any $\mathrm{x} \in \mathcal{F}$, $\mathcal{LF}_{\mathbb{S}}(\mathrm{x})$ is a nonempty closed convex set containing x as is $\mathcal{LF}(\mathrm{x})$.

To safely steer a single-integrator disk-shaped robot towards a given goal location $\mathrm{x}^* \in \mathcal{F}$ using a fixed radius sensory footprint, we propose the following "move-to-projected-goal" law,

$$\mathrm{u}(\mathrm{x}) = -k\big(\mathrm{x} - \Pi_{\mathcal{LF}_{\mathbb{S}}(\mathrm{x})}(\mathrm{x}^*)\big)\,, \quad (24)$$

where $k > 0$ is a fixed control gain, and $\Pi_{\mathcal{LF}_{\mathbb{S}}(\mathrm{x})}$ (4) is the metric projection onto the robot's sensed local free space $\mathcal{LF}_{\mathbb{S}}(\mathrm{x})$, and $\mathcal{LF}_{\mathbb{S}}(\mathrm{x})$ is assumed to be continuously updated.

Due to the nice relations between the robot's different local neighborhoods in Proposition 8 and (23), the revised "move-to-projected-goal" law for a fixed radius sensory footprint inherits all qualitative properties of the original one presented in Section 4.2.

Proposition 9. *The "move-to-projected-goal" law of a disk-shaped robot equipped with a fixed radius sensory footprint in (24) is piecewise continuously differentiable; and if Assumption 2 holds, then its unique continuously differentiable flow asymptotically steers almost all configurations in its positively invariant domain $\mathcal{F}$ towards any given goal location $\mathrm{x}^* \in \mathcal{F}$, while strictly decreasing the (squared) Euclidean distance to the goal along the way.*

Proof. The proof of the result follows patterns similar to those of Proposition 2 - Proposition 7, because of the relations between the robot's local neighborhoods in Proposition 8 and (23), and so it is omitted for the sake of brevity. ■

Navigation using a 2D LIDAR Range Scanner. We now present another practical extension of the "move-to-projected-goal" law for safe robot navigation using a 2D LIDAR range scanner in an unknown convex planar environment $\mathcal{W} \subseteq \mathbb{R}^2$ populated with convex obstacles $\mathcal{O} = \{O_1, O_2, \ldots, O_m\}$, satisfying Assumption 1. Assuming an angular scanning range of 360 degrees and a fixed radial range of $R \in \mathbb{R}_{>0}$, we model the sensory measurement of the LIDAR scanner at location $\mathrm{x} \in \mathcal{W}$ by a polar curve [42] $\rho_{\mathrm{x}} : (-\pi, \pi] \to [0, R]$, defined as,

$$\rho_{\mathrm{x}}(\theta) := \min \begin{pmatrix} R, \\ \min\Big\{ \|\mathrm{p}-\mathrm{x}\| \Big| \mathrm{p} \in \partial\mathcal{W}, \mathrm{atan2}(\mathrm{p}-\mathrm{x}) = \theta \Big\}, \\ \min\limits_i \Big\{ \|\mathrm{p}-\mathrm{x}\| \Big| \mathrm{p} \in O_i, \mathrm{atan2}(\mathrm{p}-\mathrm{x}) = \theta \Big\} \end{pmatrix}. \tag{25}$$

Here, the LIDAR sensing range R is asummed to be greater than the robot body radius r.

Suppose $\rho_i : (\theta_{l_i}, \theta_{u_i}) \to [0, R]$ is a convex curve segment of the LIDAR scan ρ_{x} (25) at location $\mathrm{x} \in \mathcal{W}$ (please refer to Appendix V in Supplementary Material for the notion of convexity in polar coordinates which we use to identify convex polar curve segments in a LIDAR scan, corresponding to the obstacle and workspace boundary), then we define the associated *line-of-sight obstacle* as the open epigraph of ρ_i whose pole is located at x [42], [7] [14]

$$L_i := \{\mathrm{x}\} \oplus \mathring{\mathrm{epi}}\rho_i = \{\mathrm{x}\} \oplus \Big\{ (\varrho\cos\theta, \varrho\sin\theta) \Big| \theta \in (\theta_{l_i}, \theta_{u_i}), \varrho > \rho_i(\theta) \Big\}, \tag{26}$$

which is an open convex set. Accordingly, we assume the availability of a sensor model $\mathcal{L}_R(\mathrm{x}) := \{L_1, L_2, \ldots, L_t\}$ that returns the list of convex line-of-sight obstacles detected by the LIDAR scanner at location x, where t denotes the number of detected obstacles and changes as a function of robot location.

Following the lines of (7) and (9), we define the robot's *line-of-sight local workspace* and *line-of-sight local free space*, illustrated in Fig. 2(right), respectively, as

$$\mathcal{LW}_{\mathcal{L}}(\mathrm{x}) := \Big\{ \mathrm{q} \in L_{ft}(\mathrm{x}) \cap \overline{B\big(\mathrm{x}, \tfrac{r+R}{2}\big)} \Big| \Big\| \mathrm{q}-\mathrm{x}+r\tfrac{\mathrm{x}-\Pi_{\overline{L}_i}(\mathrm{x})}{\|\mathrm{x}-\Pi_{\overline{L}_i}(\mathrm{x})\|} \Big\| \leq \big\| \mathrm{q}-\Pi_{\overline{L}_i}(\mathrm{x}) \big\|, \forall i \Big\}. \tag{27}$$

$$\mathcal{LF}_{\mathcal{L}}(\mathrm{x}) := \Big\{ \mathrm{q} \in \mathcal{LW}_{\mathcal{L}}(\mathrm{x}) \Big| \overline{B(\mathrm{q}, r)} \subseteq \mathcal{LW}_{\mathcal{L}}(\mathrm{x}) \Big\}, \tag{28}$$

where $L_{ft}(\mathrm{x})$ denotes the LIDAR sensory footprint at x, given by the hypograph of the LIDAR scan ρ_{x} (25) at x, i.e.,

$$L_{ft}(\mathrm{x}) := \{\mathrm{x}\} \oplus \mathrm{hyp}\rho_{\mathrm{x}} = \{\mathrm{x}\} \oplus \Big\{ (\varrho\cos\theta, \varrho\sin\theta) \Big| \theta \in (-\pi, \pi], 0 \leq \varrho \leq \rho_{\mathrm{x}}(\theta) \Big\}. \tag{29}$$

Similar to Proposition 1 and Corollary 1, we have:

Proposition 10. *For any* $\mathrm{x} \in \mathcal{F}$, $\mathcal{LW}_{\mathcal{L}}(\mathrm{x})$ *is an obstacle free closed convex subset of* $\mathcal{W}$ *and contains the robot body* $B(\mathrm{x}, r)$. *Therefore,* $\mathcal{LF}_{\mathcal{L}}(\mathrm{x})$ *is a nonempty closed convex subset of* $\mathcal{F}$ *and contains* x.

Proof. See Appendix I-E in Supplementary Material. ■

[14] Here, $\mathring{A}$ denotes the interior of a set A.

Accordingly, to navigate a fully-actuated single-integrator robot using a LIDAR scanner towards a desired goal location $\mathrm{x}^* \in \mathcal{F}$, with the guarantee of no collisions along the way, we propose the following "move-to-projected-goal" law

$$\mathrm{u}(\mathrm{x}) = -k\big(\mathrm{x} - \Pi_{\mathcal{L}\mathcal{F}_{\mathcal{L}}(\mathrm{x})}(\mathrm{x}^*)\big), \tag{30}$$

where $k > 0$ is fixed, and $\Pi_{\mathcal{L}\mathcal{F}_{\mathcal{L}}(\mathrm{x})}$ (4) is the metric projection onto the robot's line-of-sight free space $\mathcal{L}\mathcal{F}_{\mathcal{L}}(\mathrm{x})$ (28), which is assumed to be continuously updated.

We summarize important properties of the "move-to-projected-goal" law for navigation using a LIDAR scanner as:

Proposition 11. *The "move-to-projected-goal" law of a LIDAR-equipped disk-shaped robot in (30) leaves the robot's free space $\mathcal{F}$ (1) positively invariant; and if Assumption 2 holds, then its unique, continuous and piecewise differentiable flow asymptotically brings all but a mesure zero set of initial configurations in $\mathcal{F}$ to any designated goal location $\mathrm{x}^* \in \mathcal{F}$, while strictly decreasing the (squared) Euclidean distance to the goal along the way.*

Proof. See Appendix I-F in Supplementary Material. ■

As a final remark, it is useful to note that the "move-to-projected-goal" law in (30) might have discontinuities because of possible occlusions between obstacles. If there is no occlusion between obstacles in the LIDAR's sensing range, then the LIDAR scanner provides exactly the same information about obstacles as does the fixed radius sensory footprint of Section 4.3, and so the "move-to-projected-goal" law in (30) is piecewise continuously differentiable as is its version in (24). In this regard, one can avoid occlusions between obstacles by properly selecting the LIDAR's sensing range: for example, since $d(\mathrm{x}, O_i) \geq r$ for any $\mathrm{x} \in \mathcal{F}$ and $d(O_i, O_j) > 2r$ for any $i \neq j$ (Assumption 1), a conservative choice of R that prevents occlusions between obstacles is $r < R \leq 3r$.

5 Numerical Simulations

To demonstrate the motion pattern generated by our "move-to-projected-goal" law around and far away from the goal, we consider a 10×10 and a 50×10 environment cluttered with convex obstacles and a desired goal located at around the upper right corner, as illustrated in Fig. 3 and Fig. 4, respectively.[15] We present in these figures example navigation trajectories of the "move-to-projected-goal" law for different sensing and actuation modalities. We observe a significant consistency between the resulting trajectories of the "move-to-projected-goal" law and the boundary of the Voronoi diagram of the environment, where the robot balances its distance to all proximal obstacles while navigating towards its destination — a desired autonomous behaviour for many practical settings instead of following the obstacle boundary tightly. In our simulations, we

[15] For all simulations we set $r = 0.5$, $R = 2$ and $k = 1$, and all simulations are obtained through numerical integration of the associated "move-to-projected-goal" law using the `ode45` function of MATLAB. Please refer to Appendix VII in Supplementary Material and see the accompanying video submission for additional figures illustrating the navigation pattern far away from the goal for different sensing and actuation models.

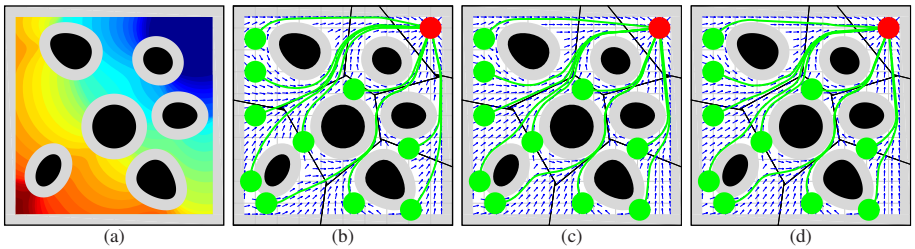

Fig. 3. (a) The Euclidean distance, $\left\|\Pi_{\mathcal{LF}(\mathrm{x})}(\mathrm{x}^*) - \mathrm{x}^*\right\|$, between the projected goal, $\Pi_{\mathcal{LF}(\mathrm{x})}(\mathrm{x}^*)$, and the global goal, x^*, for Voronoi-adjacent[9] obstacle sensing. (b-d) Example navigation trajectories of the "move-to-projected-goal" law starting at a set of initial configurations (green) towards a designated point goal (red) for different sensing models: (c) Voronoi-adjacent[9] obstacle sensing, (d) a fixed radius sensory footprint, (e) a limited range LIDAR sensor.

avoid occlusions between obstacles by properly selecting the LIDAR's sensing range, and in so doing both limited range sensing models provide the same information about the environment away from the workspace boundary and the associated "move-to-projected-goal" laws yield almost the same navigation paths. It is also useful to note that the "move-to-projected-goal" law decreases not only the Euclidean distance, $\|\mathrm{x} - \mathrm{x}^*\|$, to the goal, but also the Euclidean distance, $\left\|\Pi_{\mathcal{LF}(\mathrm{x})}(\mathrm{x}^*) - \mathrm{x}^*\right\|$, between the projected goal, $\Pi_{\mathcal{LF}(\mathrm{x})}(\mathrm{x}^*)$, and the global goal, x^*, illustrated in Fig. 3(a).

6 Conclusions

In this paper we construct a sensor-based feedback law that solves the real-time collision-free robot navigation problem in a domain cluttered with unknown but sufficiently separated and strongly convex obstacles. Our algorithm introduces a novel use of separating hyperplanes for identifying the robot's local obstacle free convex neighborhood, affording a piecewise smooth velocity command instantaneously pointing toward the metric projection of the designated goal location onto this convex set. Given sufficiently separated (Assumption 1) and appropriately "strongly" convex (Assumption 2) obstacles, we show that the resulting vector field has a smooth flow with a unique attractor at the goal location (along with the topologically inevitable saddles — at least one for each obstacle). Since all of its critical points are nondegenerate, our vector field asymptotically steers almost all configurations in the robot's free space to the goal, with the guarantee of no collisions along the way. We also present its practical extensions for two limited range sensing models. We illustrate the effectiveness of the proposed navigation algorithm in numerical simulations.

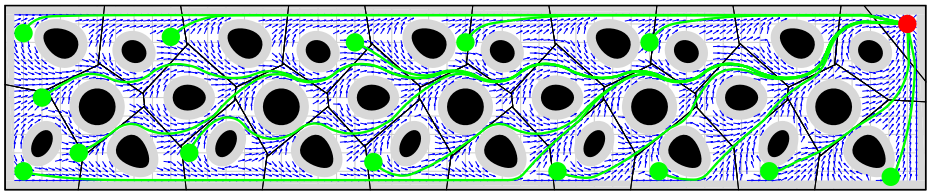

Fig. 4. Example navigation trajectories of the "move-to-projected-goal" law in (10) starting at a set of initial positions (green) far away from the goal (red).[15]

Work now in progress targets a fully smoothed version of the move-to-projected-goal law (by recourse to reference governors [43]), permitting its lift to more complicated dynamical models such as force-controlled (second-order) and underactuated systems [44]. This will enable its empirical demonstration for safe, high-speed navigation in a forest-like environments [45] and in human crowds. We are also investigating the extension of these ideas for coordinated, decentralized feedback control of multirobot swarms. More generally, we seek to identify fundamental limits on navigable environments for a memoryless greedy robotic agent with a limited range sensing capability.

Acknowlegdment. This work was supported by AFOSR under the CHASE MURI FA9550-10-1-0567.

References

1. Trautman, P., Ma, J., Murray, R.M., Krause, A.: Robot navigation in dense human crowds: Statistical models and experimental studies of humanrobot cooperation. The International Journal of Robotics Research **34**(3) (2015) 335–356
2. Henry, P., Vollmer, C., Ferris, B., Fox, D.: Learning to navigate through crowded environments. In: Robotics and Automation, IEEE International Conference on. (2010) 981–986
3. Karaman, S., Frazzoli, E.: High-speed flight in an ergodic forest. In: Robotics and Automation (ICRA), IEEE International Conference on. (2012) 2899–2906
4. Paranjape, A.A., Meier, K.C., Shi, X., Chung, S.J., Hutchinson, S.: Motion primitives and 3D path planning for fast flight through a forest. The Int. J. Robot. Res. **34**(3) (2015) 357–377
5. Wooden, D., Malchano, M., Blankespoor, K., Howardy, A., Rizzi, A.A., Raibert, M.: Autonomous navigation for BigDog. In: IEEE Int. Conf. Robot. Autom. (2010) 4736–4741
6. Johnson, A.M., Hale, M.T., Haynes, G.C., Koditschek, D.E.: Autonomous legged hill and stairwell ascent. In: Safety, Security, and Rescue Robotics (SSRR), IEEE International Symposium on. (2011) 134–142
7. Choset, H., Lynch, K.M., Hutchinson, S., Kantor, G.A., Burgard, W., Kavraki, L.E., Thrun, S.: Principles of Robot Motion: Theory, Algorithms, and Implementations. MIT Press (2005)
8. LaValle, S.M.: Planning Algorithms. Cambridge University Press, Cambridge, U.K. (2006)
9. Koditschek, D.E., Rimon, E.: Robot navigation functions on manifolds with boundary. Advances in Applied Mathematics **11**(4) (1990) 412 – 442
10. Khatib, O.: Real-time obstacle avoidance for manipulators and mobile robots. The International Journal of Robotics Research **5**(1) (1986) 90–98
11. Koditschek, D.E.: Exact robot navigation by means of potential functions: Some topological considerations. In: Robotics and Automation, IEEE International Conference on. (1987) 1–6
12. Rimon, E., Koditschek, D.E.: Exact robot navigation using artificial potential functions. Robotics and Automation, IEEE Transactions on **8**(5) (1992) 501–518
13. Lionis, G., Papageorgiou, X., Kyriakopoulos, K.J.: Locally computable navigation functions for sphere worlds. In: Robotics and Automation, IEEE Int. Conf. on. (2007) 1998–2003
14. Filippidis, I., Kyriakopoulos, K.J.: Adjustable navigation functions for unknown sphere worlds. In: Decision and Control and European Control Conference (CDC-ECC), IEEE Conference on. (2011) 4276–4281
15. Burridge, R.R., Rizzi, A.A., Koditschek, D.E.: Sequential composition of dynamically dexterous robot behaviors. The International Journal of Robotics Research **18**(6) (1999) 535–555
16. Conner, D.C., Choset, H., Rizzi, A.A.: Flow-through policies for hybrid controller synthesis applied to fully actuated systems. Robotics, IEEE Transactions on **25**(1) (2009) 136–146
17. Choset, H., Burdick, J.: Sensor-based exploration: The hierarchical generalized Voronoi graph. The International Journal of Robotics Research **19**(2) (2000) 96–125

18. Boyd, S., Vandenberghe, L.: Convex Optimization. Cambridge University Press (2004)
19. Arslan, O., Koditschek, D.E.: Exact robot navigation using power diagrams. In: Robotics and Automation (ICRA), IEEE International Conference on. (2016) 1–8
20. Aurenhammer, F.: Power diagrams: Properties, algorithms and applications. SIAM Journal on Computing **16**(1) (1987) 78–96
21. Webster, R.: Convexity. Oxford University Press (1995)
22. Ó'Dúnlaing, C., Yap, C.K.: A retraction method for planning the motion of a disc. Journal of Algorithms **6**(1) (1985) 104 – 111
23. Cortés, J., Martınez, S., Karatas, T., Bullo, F.: Coverage control for mobile sensing networks. Robotics and Automation, IEEE Transactions on **20**(2) (2004) 243–255
24. Kwok, A., Martnez, S.: Deployment algorithms for a power-constrained mobile sensor network. International Journal of Robust and Nonlinear Control **20**(7) (2010) 745–763
25. Pimenta, L.C., Kumar, V., Mesquita, R.C., Pereira, G.A.: Sensing and coverage for a network of heterogeneous robots. In: Decision and Control, IEEE Conference on. (2008) 3947–3952
26. Arslan, O., Koditschek, D.E.: Voronoi-based coverage control of heterogeneous disk-shaped robots. In: Robotics and Automation, IEEE International Conference on. (2016) 4259–4266
27. Okabe, A., Boots, B., Sugihara, K., Chiu, S.N.: Spatial Tessellations: Concepts and Applications of Voronoi Diagrams. 2nd edn. Volume 501. John Wiley & Sons (2000)
28. Haralick, R.M., Sternberg, S.R., Zhuang, X.: Image analysis using mathematical morphology. Pattern Analysis and Machine Intelligence, IEEE Transactions on **9**(4) (1987) 532–550
29. Munkres, J.: Topology. 2nd edn. Pearson (2000)
30. Kozlov, M., Tarasov, S., Khachiyan, L.: The polynomial solvability of convex quadratic programming. USSR Comp. Mathematics and Mathematical Physics **20**(5) (1980) 223–228
31. Bullo, F., Cortés, J., Martinez, S.: Distributed Control of Robotic Networks: A Mathematical Approach to Motion Coordination Algorithms. Princeton University Press (2009)
32. Rockafellar, R.: Lipschitzian properties of multifunctions. Nonlinear Analysis: Theory, Methods & Applications **9**(8) (1985) 867–885
33. Kuntz, L., Scholtes, S.: Structural analysis of nonsmooth mappings, inverse functions, and metric projections. Journal of Math. Analysis and Applications **188**(2) (1994) 346–386
34. Shapiro, A.: Sensitivity analysis of nonlinear programs and differentiability properties of metric projections. SIAM Journal on Control and Optimization **26**(3) (1988) 628–645
35. Liu, J.: Sensitivity analysis in nonlinear programs and variational inequalities via continuous selections. SIAM Journal on Control and Optimization **33**(4) (1995) 1040–1060
36. Chaney, R.W.: Piecewise C^k functions in nonsmooth analysis. Nonlinear Analysis: Theory, Methods & Applications **15**(7) (1990) 649 – 660
37. Khalil, H.K.: Nonlinear Systems. 3rd edn. Prentice Hall (2001)
38. Paternain, S., Koditschek, D.E., Ribeiro, A.: Navigation functions for convex potentials in a space with convex obstacles. IEEE Transactions on Automatic Control (submitted)
39. Holmes, R.B.: Smoothness of certain metric projections on Hilbert space. Transactions of the American Mathematical Society **184** (1973) 87–100
40. Fitzpatrick, S., Phelps, R.R.: Differentiability of the metric projection in Hilbert space. Transactions of the American Mathematical Society **270**(2) (1982) 483–501
41. Hirsch, M.W., Smale, S., Devaney, R.L.: Differential Equations, Dynamical Systems, and an Introduction to Chaos. 2nd edn. Academic Press (2003)
42. Stewart, J.: Calculus: Early Transcendentals. 7th edn. Cengage Learning (2012)
43. Kolmanovsky, I., Garone, E., Cairano, S.D.: Reference and command governors: A tutorial on their theory and automotive applications. In: American Control Conf. (2014) 226–241
44. Arslan, O., Koditschek, D.E.: Smooth extensions of feedback motion planners via reference governors. In: (submitted to) Robotics and Automation (ICRA), IEEE Int. Conf. on. (2017)
45. Vasilopoulos, V., Arslan, O., De, A., Koditschek, D.E.: Minitaur bounds home through a locally sensed artificial forest. In: (submitted to) IEEE Int. Conf. Robot. Autom. (2017)